(ChIP) coupled to pyrosequencing. Our results have revealed dynamic histone modifications in the vicinity of a subset of protein-coding genes in the human genome, which directly participate in regulation of the contraction of cardiac myocytes.

Results

Histone modifications in the heart of Dahl rats

We prepared LV myocytes from Dahl salt-sensitive rats, which are genetically intolerant to excessive salt intake (Rapp *et al.* 1989). A high-sodium diet thus induces systemic hypertension and cardiac hypertrophy in Dahl rats within a few weeks. These changes are followed within a few months by the development of CHF and death. We isolated cardiac myocytes from rats with CHF (fed a high-sodium diet) as well as from age-matched animals with a normal heart (fed a low-sodium diet), and we subjected these cells to ChIP with antibodies to acetylated histone H3 (H3Ac), acetylated histone H4 (H4Ac), histone H3 dimethylated on lysine-4 (K4DM), histone H3 trimethylated on lysine-4 (K4TM), histone H3 dimethylated on lysine-9 (K9DM), histone H3 trimethylated on lysine-9 (K9TM), histone H4 trimethylated on lysine-20 (K20TM), or histone H3 dimethylated on lysine-27 (K27DM). The ChIP products as well as cRNA prepared from the normal or failed hearts were then individually subjected to hybridization with high-density oligonucleotide microarrays (Affymetrix Rat Genome 230 2.0 GeneChip) originally developed for expression profiling of rat genes.

Pearson's correlation coefficient for the signal intensity of all probe sets with a "Present" call (by Affymetrix GCOS software) in the normal heart ($n = 13\ 914$) was 0.873 in the cRNA hybridizations for normal and failed hearts (Fig. 1), indicative of a strong correlation in the expression level of most genes between the two samples. Consistent with this observation, the signal intensity for all probe sets with a positive value in the H3Ac ChIP products from the normal heart ($n = 12\ 027$) was highly correlated between these products from normal and failed hearts ($r = 0.724$). A similar strong correlation between the two groups was observed for H4Ac.

Unexpectedly, however, despite the strong correlation ($r = 0.856$) apparent for K4DM, only a weak negative correlation ($r = -0.097$) was detected for the K4TM mark between normal and failed hearts, indicative of marked differences in the associated gene sets. Similarly, although a strong correlation was observed for K9DM ($r = 0.558$), a weak negative correlation ($r = -0.251$) was apparent for K9TM. Hybridization levels were positively correlated between normal and failed hearts for K20TM and K27DM.

Thus, among the epigenetic marks examined, K4TM and K9TM were the histone modifications most affected in heart failure. Although differences in functional roles and genomic distributions between K4DM and K4TM have been described (Santos-Rosa *et al.* 2002; Bernstein *et al.* 2005), little has been known of such differential roles for the methylation level of lysine-9 of histone H3.

K4TM and K9TM profiles in the human heart

We next attempted to identify the genomic regions associated with the K4TM and K9TM marks in human cardiac myocytes. ChIP products for K4TM or K9TM were prepared from a mixture of LV tissue specimens from four individuals with retained pumping function [LV ejection fraction (EF) of 65.5 ± 7.6%, mean ± SD] or from four individuals with CHF (LVEF of 19.8 ± 5.7%) caused by dilated cardiomyopathy (Table 1). The ChIP

Table 1 Clinical characteristics of the subjects who provided specimens for the study

	Sample ID	Disease	Age (years)	Sex	LVEF (%)
HighEF	PM 8	HVD (MSR, ASR)	59	F	65
	PM12	HVD (MSR)	73	F	58
	PM13	HVD (MS)	55	F	76
	PM14	HVD (MS)	62	F	63
CHF	LV13	DCM	52	M	17
	LV14	DCM	55	M	25
	LV18	DCM	57	M	13
	LV20	DCM	64	F	24

HVD, heart valvular disease; MS(R), mitral stenosis (and regurgitation); ASR, aortic stenosis and regurgitation; DCM, dilated cardiomyopathy; F, female; M, male.

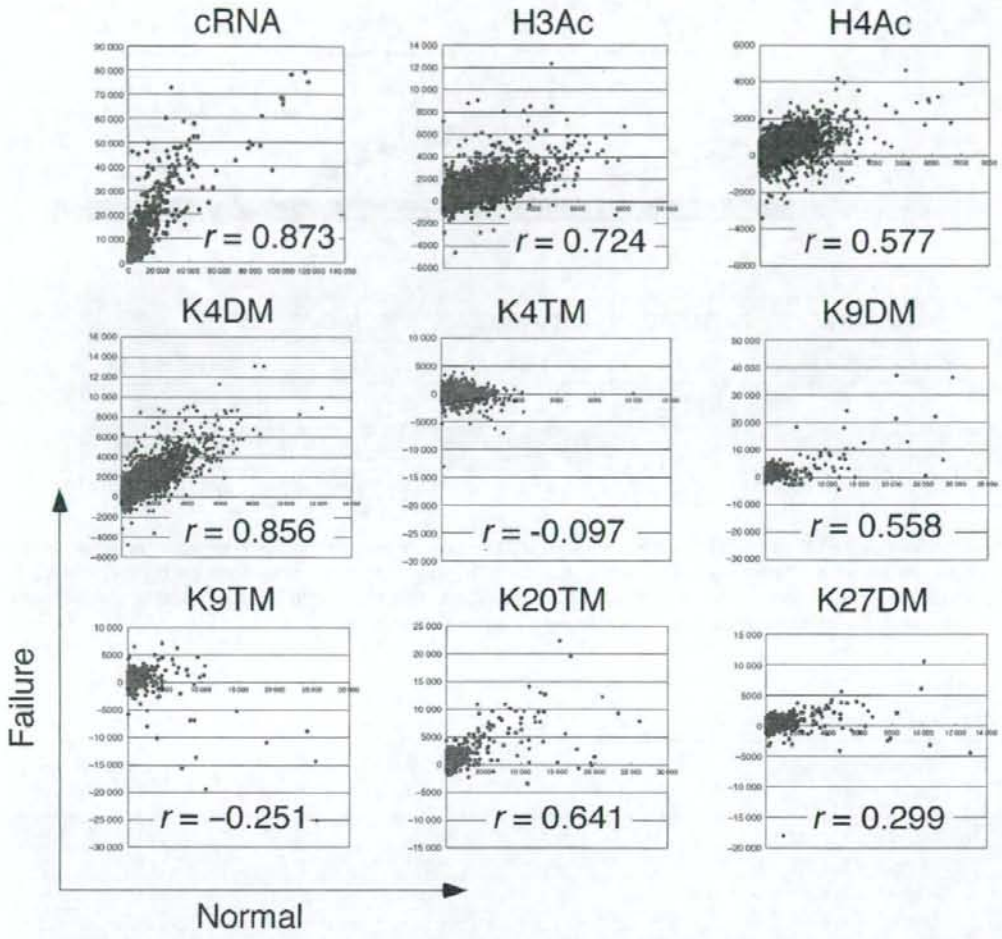

Figure 1 Comparison of epigenetic profiles between normal and failed rat hearts. The expression level of each probe set on oligonucleotide microarrays was compared between total cRNA from normal (*x* axis) or failed (*y* axis) hearts by calculation of Pearson's correlation coefficient (*r*). ChIP-on-chip data for H3Ac, H4Ac, K4DM, K4TM, K9DM, K9TM, K20TM, and K27DM are similarly compared.

products were subjected to pyrosequencing with the Genome Sequencer 20 system (Roche). In this "ChIP-to-seq" experiment, 96 069, 95 596, 116 267, and 96 734 reads were obtained for the K4TM products for specimens with retained LV ejection fraction (HighEF), the K4TM products for CHF, the K9TM products for HighEF, and the K9TM products for CHF, respectively. After quality-filtering, we isolated an average of 36 279 reads per sample, for each of which a single hit with a highest matching score was identified in the human genome sequence (the hg18 assembly of the Genome Bioinformatics Group, University of California at Santa Cruz) (Table S1 in Supporting Information). We thus focused on these reads for further analysis.

Many regions of the genome were identified in which multiple sequence reads mapped closely to each other. We therefore defined a "cluster" as a group of sequence reads localized within a distance of 1 kbp in the human genome (Fig. 2A). A total of 94 202 clusters was identified for all four samples, and 18 725 of these clusters, referred to as "high clusters," contained ≥ 2 sequence reads in ≥ 1 sample (see Table S2 in Supporting Information).

We then examined histone modification at the high clusters for specificity of the epigenetic mark (K4TM or

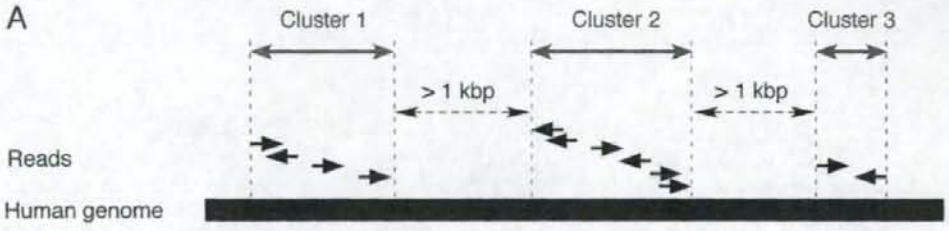

B

K4TM-HighEF	K4TM-CHF	K9TM-HighEF	K9TM-CHF	
875	21	31	24	K4TM-HighEF
	818	22	17	K4TM-CHF
		269	25	K9TM-HighEF
			229	K9TM-CHF

Figure 2 High clusters in K4TM and K9TM ChIP-to-seq data. (A) Groups of sequence reads that map to the human genome within a distance of 1 kbp are defined as "clusters," which are further denoted as "high clusters" when the read number in the cluster is ≥ 2 in ≥ 1 sample. (B) Numbers of high clusters with a read number of ≥ 5 for K4TM or K9TM in HighEF or CHF samples (shaded boxes). The numbers of such clusters shared between any pair of samples is also indicated (open boxes).

Table 2 Disease-specific high clusters

Mark	Characteristics of high clusters	Total number of high clusters	Number of high clusters close to RefSeq genes	Number of high clusters close to CpG islands
K4TM	HighEF ≥ 5, CHF ≤ 1	836	407	129
	HighEF ≤ 1, CHF ≥ 5	786	432	163
K9TM	HighEF ≥ 5, CHF ≤ 1	220	75	18
	HighEF ≤ 1, CHF ≥ 5	196	69	10

K9TM) and disease status (HighEF or CHF). Among the high clusters, 875 had ≥ 5 reads in the K4TM product for HighEF, 818 had ≥ 5 reads in the K4TM product for CHF, 269 had ≥ 5 reads in the K9TM product for HighEF, and 229 had ≥ 5 reads in the K9TM product for CHF (Fig. 2B). Only a few dozen of such high clusters were shared between any pair of samples, indicating the existence of disease-specific as well as methylation site-specific epigenetic profiles. Therefore, despite the heterogeneity in the cause of CHF (sustained systemic hypertension or dilated cardiomyopathy), both the Dahl rat and human data sets revealed a marked difference in the K4TM and K9TM epigenetic profiles between normal and failed hearts. Such specificity is further visualized for human chromosome 1 in Fig. S1 in Supporting Information. In contrast, the profile of read number per cluster was similar among the four groups of human ChIP products (see Fig. S2 in Supporting Information).

Genes mapped closely to disease-dependent clusters

We then isolated disease status-specific high clusters from the data set. A total of 836 high clusters was found to contain ≥ 5 reads in the K4TM products for HighEF but ≤ 1 read in those for CHF (HighEF-specific K4TM clusters); 407 RefSeq genes mapped to within ≤ 5 kbp of these clusters (Table 2). Similarly, 786 high clusters were found to be specific for K4TM and CHF (≤ 1 read in the K4TM products for HighEF but ≥ 5 reads in those for CHF). Smaller numbers of disease-dependent clusters were identified for the K9TM mark (220 HighEF-specific and 196 CHF-specific). These disease-dependent clusters

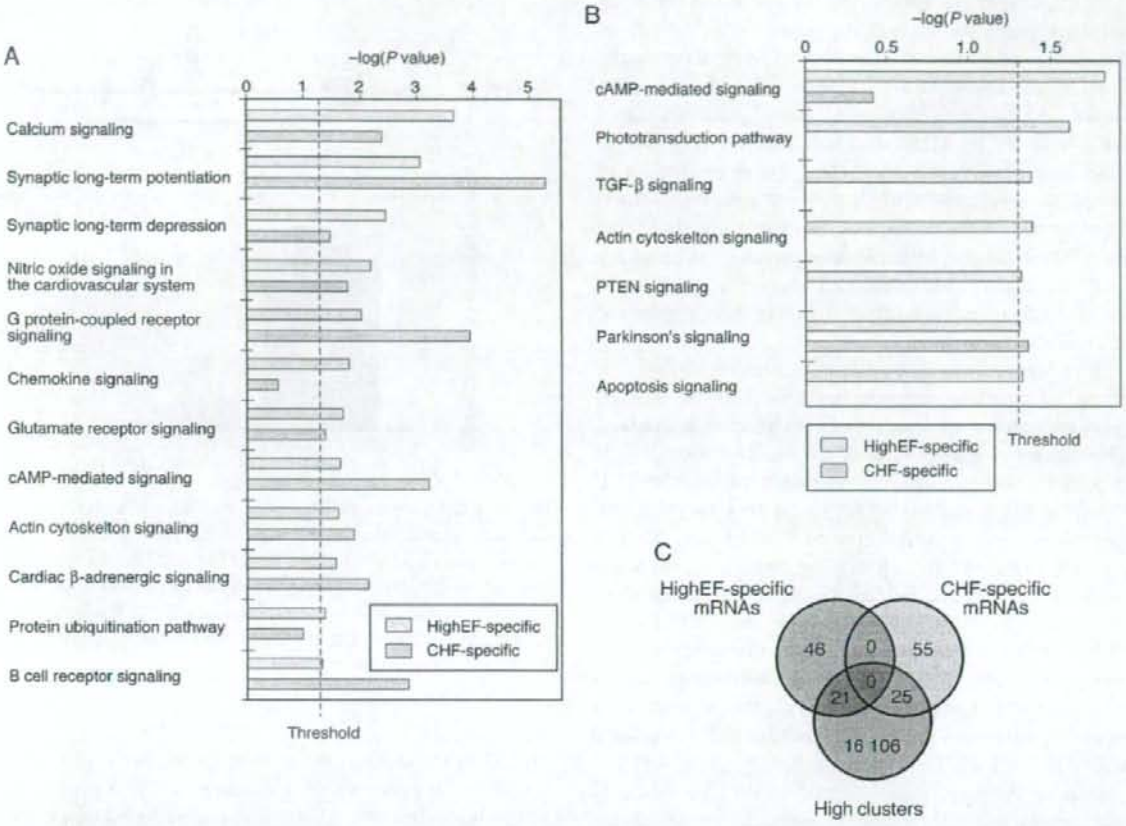

Figure 3 Analysis of genes that map in the vicinity of disease-dependent high clusters. (A) Canonical signaling pathways overrepresented in the HighEF-specific or CHF-specific high clusters for the K4TM ChIP products are listed with the corresponding −log(*P* value) score. (B) Canonical signaling pathways overrepresented in the HighEF-specific or CHF-specific high clusters for the K9TM ChIP products are listed with the corresponding −log(*P* value) score. (C) Venn diagram for comparison of transcripts associated specifically with HighEF or CHF status and those encoded by genes that map within a distance of < 5 kbp relative to a high cluster.

were widely distributed throughout human chromosomes and showed little overlap (see Fig. S3 in Supporting Information).

We examined whether the protein products of RefSeq genes that mapped in the vicinity (a distance of ≤ 5 kbp) of disease-dependent clusters function in canonical intracellular signaling pathways with the use of Ingenuity Pathway Analysis software (Ingenuity Systems; http://www.ingenuity.com). Analysis of the RefSeq genes associated with the disease-dependent K4TM clusters identified 12 canonical pathways that were significantly overrepresented ($P < 0.05$, Fisher's exact test) in HighEF-specific clusters and 20 pathways overrepresented in CHF-specific clusters. Many of the pathways ($n = 10$) were overrepresented in both HighEF-K4TM and CHF-K4TM clusters, almost all of which (including those for calcium signaling, synaptic long-term regulation, and nitric oxide signaling) are related to cardiac function (Fig. 3A).

Consistent with the disease-dependent selection of the clusters, the HighEF-associated and CHF-associated genes were distinct even within the same pathways. The canonical pathway for synaptic long-term potentiation, for example, contains the products of eight HighEF-associated and 12 CHF-associated genes, the interactions among which are shown in Fig. S4 in Supporting Information. Although genes corresponding to the calmodulin complex are present in both gene sets, these genes differ between the HighEF set (*CALM1*) and the CHF set (*CALM3*).

In addition to the proteins of the canonical signaling pathways, many products of the genes in the vicinity of disease-dependent high clusters for K4TM are functionally or physically networked. One such network comprises 34 proteins, 18 of which are encoded by HighEF-associated genes and 16 by CHF-associated genes (Fig. S5 in Supporting Information). Again, the genes for some complexes associated with both gene sets are distinct; those for the ATPase complex, for instance, include that for ATP1B1 in the HighEF-associated set and that for ATP5C1 in the CHF-associated set. Gene products in this network are substantially enriched in those implicated in cardiovascular disease.

In contrast to the K4TM-specific clusters, only a few canonical signaling pathways are linked to the RefSeq genes localized in the vicinity of K9TM-specific clusters. This difference is due in part to the small number of high clusters that contain disease-dependent reads for K9TM. Whereas the numbers of high clusters for HighEF specimens were similar between K4TM and K9TM products ($n = 6547$ and 5594, respectively), the numbers of disease-dependent clusters for the K9TM mark were only approximately 25% of those for the K4TM mark (Table 2). Seven canonical signaling pathways were over-represented ($P < 0.05$, Fisher's exact test) in the genes associated with the HighEF-K9TM clusters, whereas only one such pathway was overrepresented in those associated with the CHF-K9TM clusters (Fig. 3B). The network containing the most disease-dependent K9TM-associated gene products is centered on transforming growth factor β1 (TGFB1) and the tumor suppressor p53 (TP53), implicating K9TM-related regulation in cell death in the heart (see Fig. S6 in Supporting Information).

Our analysis thus revealed differential regulation of K4TM modification for genes related to cardiac function. To examine whether such epigenetic regulation plays a direct role in gene transcription, we performed gene expression profiling with Human Genome U133 Plus 2.0 arrays (Affymetrix) for the individual specimens (four for HighEF and four for CHF) used in the ChIP experiments. From the data obtained for 54 675 probe sets and the eight specimens, we selected HighEF-specific probe sets according to the following criteria: (i) the ratio of the mean expression level between HighEF and CHF was ≥ 3, and (ii) the mean expression level in HighEF was ≥ 10 arbitrary units (U). These criteria resulted in the isolation of 67 probe sets (see Table S3 in Supporting Information). CHF-specific probe sets were also selected on the basis of a CHF/HighEF ratio for mean expression level of ≥ 3 and a mean expression level in CHF of ≥ 10 U, resulting in the identification of 80 probe sets (see Table S4 in Supporting Information). A total of

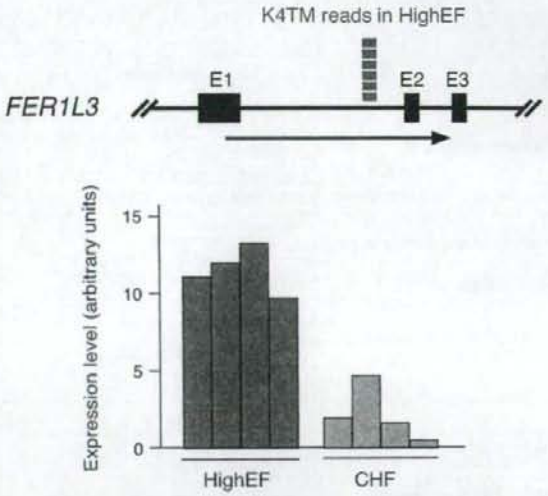

Figure 4 Epigenetic profile and mRNA abundance for *FER1L3*. Six sequence reads were selectively identified in the first intron of the *FER1L3* gene for the K4TM ChIP products of the HighEF sample (upper panel). E, exon. Consistent with this epigenetic profile, the amount of *FER1L3* mRNA was higher in the HighEF specimens than in the CHF specimens, as judged from the microarray data (lower panel).

16 152 of the transcripts measured with the U133 Plus 2.0 arrays mapped within a distance of ≤ 5 kbp relative to the high clusters. A Venn diagram revealed that only 21 probe sets were shared between the HighEF-specific and high cluster–associated transcripts, whereas 25 probe sets were shared between the CHF-specific and high cluster–associated transcripts (Fig. 3C). The K4TM mark has been found to map preferentially to the transcription start sites of active genes (Bernstein *et al.* 2005). Although a typical correlation between the K4TM modification and selective gene expression was apparent for a subset of genes (Fig. 4), our results suggest that this dynamic epigenetic regulation in the heart may not always directly participate in transcriptional regulation of neighboring genes.

Discussion

In the present study, we have revealed heart failure–dependent changes in the epigenetic profiles for K4TM and K9TM marks. The antibodies used in this study have been utilized in other reports for ChIP experiments, with those for K4TM and K9TM being especially employed in a genome-wide epigenetic profiling (Pokholok *et al.* 2005; Vakoc *et al.* 2006). Although it is difficult to

extensively verify our data in this study (because of the lack of knowledge in epigenetic profiles in heart), our ChIP procedure could faithfully confirm the epigenetic data demonstrated in previous studies [You *et al.* have, for instance, revealed that an apicidin treatment decreases the K4TM level while increases the K9TM level in the exon 1 of *DNMT1* in HeLa cells (You *et al.* 2008), and we could observe similar changes in the same experiment (data not shown)], supporting the reliability of our ChIP procedures.

Despite increasing evidence for a role of histone acetylation-deacetylation in the development of cardiac hypertrophy and heart failure, little information has been available for other histone modifications in these conditions (Illi *et al.* 2005; Phan *et al.* 2005; Bingham *et al.* 2007). Given the marked differences between the profiles of dimethylation and trimethylation for both K4 and K9 sites of histone H3, such trimethylation is likely under strict regulation in failed hearts.

The genes positioned close to the K4TM or K9TM marks were highly enriched in those that encode components of signaling pathways related to cardiac function. The HighEF-specific K4TM modification was, for instance, associated with *RYR2*, *CACNA2D1*, and *CACNB2* genes, the products of which directly participate in the regulation of intracellular calcium concentration and in muscle contraction (Cataldi *et al.* 1999; Marx *et al.* 2000). However, such disease-dependent histone methylation was not always linked to the induction or repression of neighboring genes. The expression level of the above three genes thus did not differ significantly between HighEF and CHF specimens (data not shown). Furthermore, only ~30% of HighEF- or CHF-specific transcripts were derived from genes associated with disease-dependent K4TM or K9TM modification (Fig. 3C). Consistent with such observations, the expression ratio for probe sets between normal and failed hearts of Dahl rats was not significantly correlated with the intensity ratio for any of the examined histone modifications, including H3Ac and H4Ac (data not shown). Therefore, despite the marked association between disease status and both transcript abundance and a subset of histone modifications, none of the latter can directly account for the former.

The epigenetic changes associated with heart failure may regulate gene transcription not through a single modification but through a combination of various marks (the "histone code" hypothesis) (Strahl & Allis 2000). The disease-dependent epigenetic changes also may alter the conformation of chromosomes, inducing an open or closed chromatin structure that indirectly affects the targets of subsequent regulation, such as the binding of transcription factors or additional chromatin remodeling. The subsequent regulation step would then play an important role in transcription of neighboring genes. In either case, our epigenetic profiles should facilitate further investigations into the roles of epigenetic changes in the development of heart failure.

Experimental procedures

ChIP-on-chip experiments

Dahl salt-sensitive rats (Japan SLC) at 6 weeks of age were maintained on a low-sodium diet (0.3% NaCl) or switched to a high-sodium diet (8% NaCl); the latter animals developed heart failure, as detected by echocardiography, after 13 weeks, as described previously (Ueno *et al.* 2003). ChIP products were prepared from the LV myocytes of 19-week-old Dahl rats with antibodies specific to H3Ac (Upstate, #17-245), H4Ac (Upstate, #17-229), K4DM (Abcam, #ab7766), K4TM (Abcam, #ab8580), K9DM (Upstate, #07-441), K9TM (Upstate, #07-442), K20TM (Abcam, #ab9053) or K27DM (Upstate, #07-452). The products were amplified by T7 RNA polymerase and subjected to hybridization with Affymetrix Rat Genome 230 2.0 microarrays as described previously (Takayama *et al.* 2007). Total genomic DNA (Pre-ChIP) and cRNA prepared from the LV tissue were also hybridized to the same arrays. The mean expression intensity of all probe sets was set to 500 U in each hybridization, and the fluorescence intensity of each test gene was normalized accordingly. Microarray data for rat and human hearts are available at the Gene Expression Omnibus web site (http://www.ncbi.nlm.nih.gov/geo) under the accession numbers GSE8341 and GSE8331, respectively. For the ChIP data, the signal intensity of each probe set in the Pre-ChIP analysis was then subtracted from that of the corresponding probe set in each ChIP experiment.

ChIP-to-seq experiments

All clinical specimens were obtained with written informed consent, and the study was approved by the ethics committees of Jichi Medical University and Hayama Heart Center. ChIP products were prepared from pooled samples for HighEF or CHF (each derived from four specimens) with antibodies to K4TM or K9TM. The products were converted to cRNA and amplified as described above for ChIP-on-chip experiments. The cRNA was then used to generate double-stranded DNA, which was subjected to pyrosequencing with a Genome Sequencer 20 system (Roche Diagnostics). Keypass wells occupied 82.7% to 87.0% of original Raw wells. Homology searches with the BLAST program were performed against the human genome sequence (the hg18 assembly) for each readout with the following parameter set: –e 2e-19 –v 50 –b 500 –T F –F F –m 8.

Acknowledgements

This work was supported in part by a Grant-in-Aid for Scientific Research on Priority Areas (C) "Medical Genome Science" from the

Ministry of Education, Culture, Sports, Science and Technology of Japan and by a grant (#04C7) from Salt Science Research Foundation (Tokyo, Japan).

References

Bernstein, B.E., Kamal, M., Lindblad-Toh, K., Bekiranov, S., Bailey, D.K., Huebert, D.J., McMahon, S., Karlsson, E.K., Kulbokas, E.J. 3rd, Gingeras, T.R., Schreiber, S.L. & Lander, E.S. (2005) Genomic maps and comparative analysis of histone modifications in human and mouse. *Cell* **120**, 169–181.

Bingham, A.J., Ooi, L., Kozera, L., White, E. & Wood, I.C. (2007) The repressor element 1-silencing transcription factor regulates heart-specific gene expression using multiple chromatin-modifying complexes. *Mol. Cell. Biol.* **27**, 4082–4092.

Braunwald, E. (1997) Shattuck lecture—cardiovascular medicine at the turn of the millennium: triumphs, concerns, and opportunities. *N. Engl. J. Med.* **337**, 1360–1369.

Cataldi, M., Secondo, A., D'Alessio, A., Taglialatela, M., Hofmann, F., Klugbauer, N., Di Renzo, G. & Annunziato, L. (1999) Studies on maitotoxin-induced intracellular $Ca^{(2+)}$ elevation in Chinese hamster ovary cells stably transfected with cDNAs encoding for L-type $Ca^{(2+)}$ channel subunits. *J. Pharmacol. Exp. Ther.* **290**, 725–730.

Gusterson, R.J., Jazrawi, E., Adcock, I.M. & Latchman, D.S. (2003) The transcriptional co-activators CREB-binding protein (CBP) and p300 play a critical role in cardiac hypertrophy that is dependent on their histone acetyltransferase activity. *J. Biol. Chem.* **278**, 6838–6847.

Iezzi, S., Di Padova, M., Serra, C., Caretti, G., Simone, C., Maklan, E., Minetti, G., Zhao, P., Hoffman, E.P., Puri, P.L. & Sartorelli, V. (2004) Deacetylase inhibitors increase muscle cell size by promoting myoblast recruitment and fusion through induction of follistatin. *Dev. Cell* **6**, 673–684.

Illi, B., Scopece, A., Nanni, S., Farsetti, A., Morgante, L., Biglioli, P., Capogrossi, M.C. & Gaetano, C. (2005) Epigenetic histone modification and cardiovascular lineage programming in mouse embryonic stem cells exposed to laminar shear stress. *Circ. Res.* **96**, 501–508.

James, M.A., Saadeh, A.M. & Jones, J.V. (2000) Wall stress and hypertension. *J. Cardiovasc. Risk* **7**, 187–190.

Kuwahara, K., Saito, Y., Ogawa, E., Takahashi, N., Nakagawa, Y., Naruse, Y., Harada, M., Hamanaka, I., Izumi, T., Miyamoto, Y., Kishimoto, I., Kawakami, R., Nakanishi, M., Mori, N. & Nakao, K. (2001) The neuron-restrictive silencer element-neuron-restrictive silencer factor system regulates basal and endothelin 1-inducible atrial natriuretic peptide gene expression in ventricular myocytes. *Mol. Cell. Biol.* **21**, 2085–2097.

Marx, S.O., Reiken, S., Hisamatsu, Y., Jayaraman, T., Burkhoff, D., Rosemblit, N. & Marks, A.R. (2000) PKA phosphorylation dissociates FKBP12.6 from the calcium release channel (ryanodine receptor): defective regulation in failing hearts. *Cell* **101**, 365–376.

Phan, D., Rasmussen, T.L., Nakagawa, O., McAnally, J., Gottlieb, P.D., Tucker, P.W., Richardson, J.A., Bassel-Duby, R. & Olson, E.N. (2005) BOP, a regulator of right ventricular heart development, is a direct transcriptional target of MEF2C in the developing heart. *Development* **132**, 2669–2678.

Pokholok, D.K., Harbison, C.T., Levine, S., Cole, M., Hannett, N.M., Lee, T.I., Bell, G.W., Walker, K., Rolfe, P.A., Herbolsheimer, E., Zeitlinger, J., Lewitter, F., Gifford, D.K. & Young, R.A. (2005) Genome-wide map of nucleosome acetylation and methylation in yeast. *Cell* **122**, 517–527.

Rapp, J.P., Wang, S.M. & Dene, H. (1989) A genetic polymorphism in the renin gene of Dahl rats cosegregates with blood pressure. *Science* **243**, 542–544.

Santos-Rosa, H., Schneider, R., Bannister, A.J., Sherriff, J., Bernstein, B.E., Emre, N.C., Schreiber, S.L., Mellor, J. & Kouzarides, T. (2002) Active genes are tri-methylated at K4 of histone H3. *Nature* **419**, 407–411.

Strahl, B.D. & Allis, C.D. (2000) The language of covalent histone modifications. *Nature* **403**, 41–45.

Takayama, K., Kaneshiro, K., Tsutsumi, S., Horie-Inoue, K., Ikeda, K., Urano, T., Ijichi, N., Ouchi, Y., Shirahige, K., Aburatani, H. & Inoue, S. (2007) Identification of novel androgen response genes in prostate cancer cells by coupling chromatin immunoprecipitation and genomic microarray analysis. *Oncogene* **26**, 4453–4463.

Ueno, S., Ohki, R., Hashimoto, T., Takizawa, T., Takeuchi, K., Yamashita, Y., Ota, J., Choi, Y.L., Wada, T., Koinuma, K., Yamamoto, K., Ikeda, U., Shimada, K. & Mano, H. (2003) DNA microarray analysis of *in vivo* progression mechanism of heart failure. *Biochem. Biophys. Res. Commun.* **307**, 771–777.

Vakoc, C.R., Sachdeva, M.M., Wang, H. & Blobel, G.A. (2006) Profile of histone lysine methylation across transcribed mammalian chromatin. *Mol. Cell. Biol.* **26**, 9185–9195.

You, J.S., Kang, J.K., Lee, E.K., Lee, J.C., Lee, S.H., Jeon, Y.J., Koh, D.H., Ahn, S.H., Seo, D.W., Lee, H.Y., Cho, E.J. & Han, J.W. (2008) Histone deacetylase inhibitor apicidin downregulates DNA methyltransferase 1 expression and induces repressive histone modifications via recruitment of corepressor complex to promoter region in human cervix cancer cells. *Oncogene* **27**, 1376–1386.

Zhang, C.L., McKinsey, T.A., Chang, S., Antos, C.L., Hill, J.A. & Olson, E.N. (2002) Class II histone deacetylases act as signal-responsive repressors of cardiac hypertrophy. *Cell* **110**, 479–488.

Received: 26 June 2008
Accepted: 10 October 2008

Supporting Information/Supplementary materials

The following Supporting Information can be found in the online version of the article:

Figure S1 Distribution of K4TM and K9TM marks on chromosome 1.

Figure S2 Distribution of read number per cluster in ChIP products.

Figure S3 Chromosome distribution of disease-specific high clusters.

Figure S4 Protein complexes in the synaptic long-term potentiation pathway in Fig. 3A are colored red or green on the basis of whether the corresponding genes are associated with HighEF-specific or CHF-specific high clusters for K4TM, respectively.

Figure S5 Interaction map for a protein network that contains the products of 18 and 16 genes associated with the HighEF-specific and CHF-specific high clusters for K4TM, respectively.

Figure S6 Network for the products of genes that mapped in the vicinity of K9TM high clusters.

Table S1 Output of pyrosequencing.

Table S2 High clusters identified in the heart specimens.

Table S3 Expression intensity of HighEF-specific probe sets.

Table S4 Expression intensity of CHF-specific probe sets.

Additional Supporting Information may be found in the online version of the article.

Please note: Wiley-Blackwell are not responsible for the content or functionality of any supporting information supplied by the authors. Any queries (other than missing material) should be directed to the corresponding author for the article.

Environ Health Prev Med (2008) 13:25–29
DOI 10.1007/s12199-007-0007-8

Epigenetic abnormalities in cardiac hypertrophy and heart failure

Hiroyuki Mano

Received: 23 June 2007 / Accepted: 4 August 2007 / Published online: 11 December 2007

Abstract Epigenetics refers to the heritable regulation of gene expression through modification of chromosomal components without an alteration in the nucleotide sequence of the genome. Such modifications include methylation of genomic DNA as well as acetylation, methylation, phosphorylation, ubiquitination, and SUMOylation of core histone proteins. Recent genetic and biochemical analyses indicate that epigenetic changes play an important role in the development of cardiac hypertrophy and heart failure, with dysregulation in histone acetylation status, in particular, shown to be directly linked to an impaired contraction ability of cardiac myocytes. Although such epigenetic changes should eventually lead to alterations in the expression of genes associated with the affected histones, little information is yet available on the genes responsible for the development of heart failure. Current efforts of our and other groups have focused on deciphering the network of genes which are under abnormal epigenetic regulation in failed hearts. To this end, coupling chromatin immunoprecipitation to high-throughput profiling systems is being applied to cardiac myocytes in normal as well as affected hearts. The results of these studies should not only improve our understanding of the molecular basis for cardiac hypertrophy/heart failure but also provide essential information that will facilitate the development of new epigenetics-based therapies.

H. Mano (✉)
Division of Functional Genomics, Jichi Medical University,
3311-1 Yakushiji, Shimotsuke, Tochigi 329-0498, Japan
e-mail: hmano@jichi.ac.jp

Keywords Cardiac hypertrophy · Chromatin immunoprecipitation · Heart failure · Histone acetylation · Subtraction

What is "epigenetics"?

The eukaryotic genome is tightly compacted as a result of its association with highly conserved histone proteins. The interaction of stretches of genomic DNA with core histone proteins (two molecules each of H2A, H2B, H3, and H4) thus results in the formation of nucleosomes, which are the basic structural units of chromatin. The further association of histone H1 and other proteins with nucleosomes strengthens the compaction and gives rise to the highly ordered, condensed structure of the chromosome (Fig. 1). The interaction of genomic DNA with these chromosomal proteins greatly influences the access of transcriptional factors to their target DNA sequences and thereby regulates transcriptional activity.

"Epigenetics" refers to the heritable regulation of gene expression through the modification of chromosomal components without an alteration in the nucleotide sequence of the genome [1]. Several such modifications have been linked to the regulation of gene expression, including methylation of genomic DNA as well as acetylation, methylation, phosphorylation, ubiquitination, and sumoylation of histone proteins (Fig. 1).

Core histones have an amino-terminal tail that protrudes from the chromatin fiber and which is believed to interact with DNA or other histone or modulatory proteins. Lysine and arginine residues within this tail are the main targets for histone modification. Lysine-9 in histone H3 (H3-K9), for example, becomes methylated or acetylated in response to a variety of signals. In general, the acetylation of

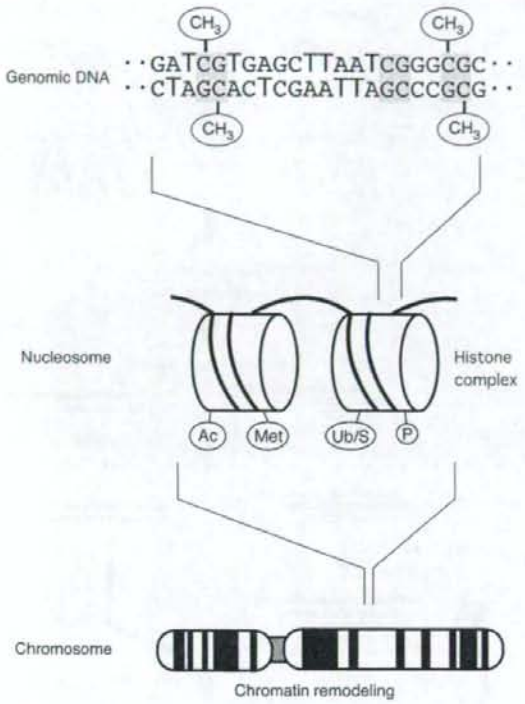

Fig. 1 Epigenetic changes at different levels of chromatin structure. CpG sites within genomic DNA undergo methylation, and core histones in nucleosomes undergo acetylation (*Ac*), methylation (*Met*), ubiquitination (*Ub*), sumoylation (*S*), or phosphorylation (*P*). Higher order chromatin structure is also dynamically modified by chromatin-remodeling complexes

histones is associated with the induction of gene expression (Fig. 2). The acetylation of histone tails is thought to neutralize the positive charge of lysine residues and thereby to induce a decondensation of chromatin structure. The resulting open architecture of the chromosome allows transcriptional factors to access their binding sites in genomic DNA and to activate transcription. However, the same histone modification has been associated with seemingly diverse outputs in a context-dependent manner. The existence of a "histone code" has thus been proposed, with a combination of histone modifications – and not only one – supposedly specifying the outcome in terms of gene expression [2]. However, this hypothesis has been challenged by recent data [3].

The acetylation of histone tails is mediated by histone acetyltransferases (HATs), whose activity in cells is rapidly counteracted by that of histone deacetylases (HDACs) [4]. The turnover time of histone acetylation in cells is thus as short as a few minutes [5]. The importance of histone acetylation in the regulation of gene expression has been demonstrated for a variety of cellular processes, including

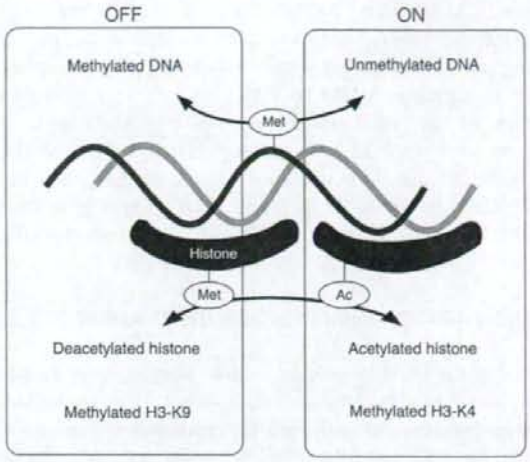

Fig. 2 Epigenetic changes and transcriptional activity. Suppression of gene expression (*OFF*) is correlated with the methylation (*Met*) of genomic DNA, deacetylation of histones, and methylation of H3-K9. In contrast, activation of gene expression (*ON*) is associated with unmethylated genomic DNA, acetylated (*Ac*) histones, and methylated H3-K4

cell differentiation, cell cycle progression, DNA repair, and carcinogenesis [6, 7].

Epigenetic status in cardiac myocytes

The regulation of histone acetylation has been shown to be linked to cardiac hypertrophy. The HAT activity of CREB-binding protein (CBP) and p300 is thus required for the induction of hypertrophic changes in cardiac muscle cells by phenylephrine [8]. Consistent with this observation, the inhibition of HDAC activity results in an increase in the size of muscle cells [9]. Furthermore, class II HDACs (HDAC4, -5, -7, and -9) suppress cardiac hypertrophy, in part by binding to and inhibiting the activity of myocyte enhancer factor 2 (MEF2) [10]. In contrast, however, HDAC2 together with Hop, a homeodomain protein, was found to promote cardiac hypertrophy in vivo in a manner sensitive to systemic administration of the HDAC inhibitor trichostatin A (TSA) [11]. Moreover, HDAC inhibitors prevent hypertrophy and sarcomere organization in cultured cardiac myocytes [12], which is suggestive of a positive role for HDACs in cardiac hypertrophy.

These seemingly discrepant findings may be attributable either to differential actions of different classes of HDACs (and, possibly, of HATs) with regard to myocyte hypertrophy or to a dissociation between the deacetylase activity of HDACs and a pro-hypertrophic function [10]. Clarification of the role of HATs and HDACs in hypertrophy

would be facilitated by the identification of the genes targeted by these enzymes during the induction of hypertrophic changes. Little is known, however, of the genes regulated by HATs or HDACs in myocytes. Induction of the atrial natriuretic peptide (ANP) gene is associated with the acetylation of histones (H3 and H4) located in the 3′ untranslated region of the gene [13]. Histones bound to the β-myosin heavy chain gene have also been shown to be targeted by HATs in myocytes [10].

Differential chromatin scanning (DCS) method

Given the essential role of histone acetylation in cardiac hypertrophy, it is important that the genes or genome regions bound to histones with such differential modifications be identified. Chromatin immunoprecipitation (ChIP) coupled with hybridization to genome tiling microarrays ("ChIP-on-chip" experiments) has been used to screen for those genes under epigenetic regulation [14–16]. However, an extensive mapping of ChIP products on the human genome has been hampered by insufficient information on human genome annotation. Furthermore, hybridization of genome-derived fragments to microarrays is prone to non-specific signals that partly represent the GC contents of the fragments.

To effectively isolate genome fragments with differential epigenetic regulation, we have developed a novel "DCS" method which basically couples ChIP to subtraction PCR [17, 18]. The DCS procedure is schematically shown in Fig. 3. Following the cross-linking of DNA to histones through the use of formaldehyde, both tester and driver cells are separately lysed and subjected to mild DNA shearing by sonication for a short period. Complexes of DNA and acetylated histones are then specifically immunoprecipitated with antibodies to acetylated histone H3, after which the DNA fragments are released from such complexes into solution.

The nonspecific binding of residual RNA is then minimized by treating the DNA solution with RNase A, and the DNA fragments are then blunt-ended. The DNA is digested maximally with *Rsa*I to obtain fragments with a relatively uniform size of several hundred base pairs. A TAG adaptor is ligated to both ends of the DNA fragments, and subsequent PCR amplification with a TAG primer yields amplicons with an *Xma*I/*Sma*I site at each end.

The tester DNA is then digested with *Xma*I (thereby generating cohesive ends), whereas the driver DNA is digested with *Sma*I (generating blunt ends). The tester DNA is ligated with the first subtraction adaptor [19] at its cohesive ends and is then annealed to an excess amount of the driver DNA. Under this condition, DNA fragments present only in the tester sample undergo self-annealing and thereby generate a binding site for the first subtraction

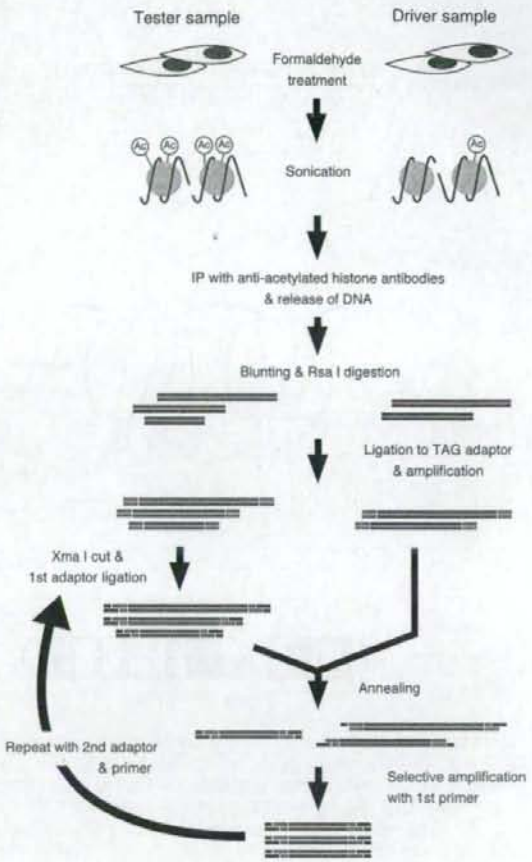

Fig. 3 The differential chromatin scanning (DCS) method. DNA fragments bound to acetylated (*Ac*) histones are purified by immunoprecipitation (*IP*) and subjected to TAG adaptor ligation (*green bars*) and PCR amplification. The tester DNA is then digested with *Xma*I, ligated to the first subtraction adaptor (*red bars*), and annealed with an excess amount of the driver DNA. Given that only the tester-specific fragments self-anneal, PCR with the first subtraction primer selectively amplifies these fragments. The products are subjected to a second round of subtraction PCR with the second subtraction adaptor and primer to ensure the fidelity of the subtraction. Reproduced from Kaneda et al. [17]

primer at both ends. Subsequent PCR amplification with this primer thus selectively amplify the tester-specific DNA fragments [17].

To exclude DNA fragments that possess endogenous (probably nonspecific) binding sites for the first subtraction primer, we then digest the first subtraction products with *Xma*I and ligate the resulting molecules with the second subtraction adaptor. A second round of subtraction amplification is then performed with the second subtraction primer, yielding DNA fragments that are associated with acetylated histones, specifically in the tester cells [17].

To verify the fidelity of DCS, we attempted to isolate genome fragments which are the targets of HDAC in cardiac myocytes. A rat cardiomyocyte cell line, H9C2, was treated with TSA and was used as the tester, while the cells without the TSA treatment was used as the driver. Differential chromatin scanning was applied to this pair of cells and subsequently identified hundreds of genome fragments that could be immunoprecipitated by antibodies to acetylated histones only in the tester cells.

Some of the clones thus identified correspond to loci within or close to rat genes whose products function in intracellular calcium mobilization or antioxidant processes. One such clone, H9C2T-2_D09, mapped to a region encompassing intron 21 and exon 22 of *Itpr3* (Fig. 4a), which encodes a receptor for inositol 1,4,5-trisphosphate that plays an important role in Ca^{2+}-mediated signal transduction [18]. The cytosolic concentration of Ca^{2+} directly regulates muscle contraction and cardiac rhythm and is a determinant of myocyte hypertrophy and heart failure [20]. The amount of the genomic fragment corresponding to the H9C2T-2_D09 clone was 6.6-fold greater in the ChIP product of TSA-treated cells than in that of untreated cells (Fig. 4b), indicating that the extent of histone acetylation in this region of the genome of the tester cells was 6.6-fold that in the driver cells. Furthermore, inhibition of HDAC activity was accompanied by an increase in the amount of *Itpr3* mRNA [18] (Fig. 4c). These data suggest that HDAC actively deacetylates a chromosomal region corresponding to *Itpr3* and thereby suppresses the transcriptional activity of the gene.

To visualize directly the genome-wide distribution of HDAC targets, we mapped the DCS genomic clones whose chromosomal positions were known to rat chromosome figures (Fig. 5). The HDAC targets were distributed widely throughout the rat genome, although some "hot spots" for deacetylation were apparent. For example, seven of the DCS clones mapped to chromosomal position 5q36, and detailed mapping revealed that all of these clones were located within a region spanning 27 Mbp. It is thus possible that regional alterations of chromatin structure result in coordinated transcriptional regulation of genes within the affected region.

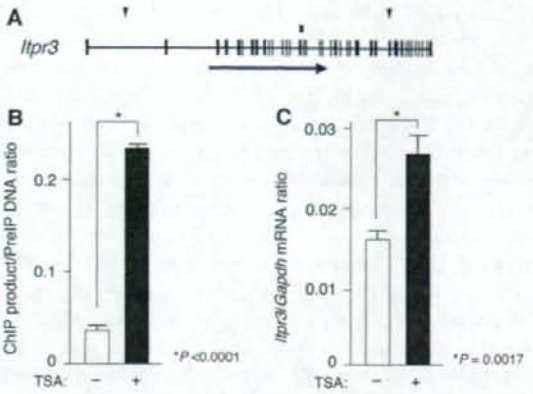

Fig. 4 Identification of *Itpr3* as a target of histone deacetylase (HDAC) in cardiomyocytes. **a** One of the DCS clones (H9C2T-2_D09; *red rectangle*) was mapped to chromosome 20p12, spanning intron 21 and exon 22 of *Itpr3*. Exons are denoted by *black boxes*, the *arrow* indicates the direction of transcription, and *blue triangles* depict distance markers separated by 50 kbp. **b** Chromatin immunoprecipitates were prepared from H9C2 cells treated (+) or not (−) with 300 n*M* inhibitor trichostatin A (TSA) for 24 h. The amount of DNA corresponding to the H9C2T-2_D09 sequence in each chromatin immunoprecipitation (*ChIP*) product relative to that in the corresponding original sample before immunoprecipitation (*PreIP*) was then determined by real-time PCR. **c** The amount of *Itpr3* mRNA relative to that of *Gapdh* mRNA in H9C2 cells treated or not with TSA was determined by quantitative reverse transcription (RT)-PCR. All data are means ± SD of triplicates from representative experiments that were performed at least twice. *P* values for the indicated comparisons were determined by Student's *t* test. Reproduced from Kaneda et al. [18]

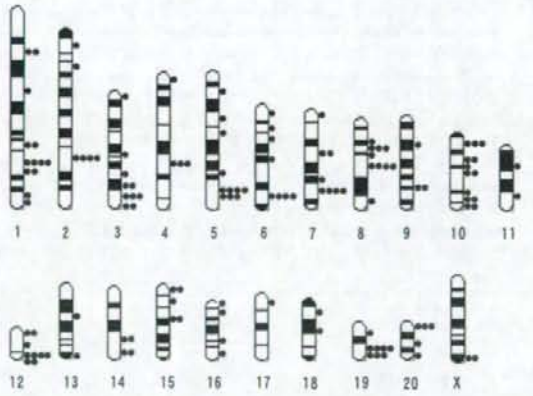

Fig. 5 Chromosomal distribution of HDAC targets. The genome fragments (*red dots*) isolated by the DCS method were mapped to rat chromosomes. Reproduced from Kaneda et al. [18]

Future directions

As described herein, cells manifest numerous types of epigenetic modifications, including acetylation and methylation, on core histone proteins. Although the results of biochemical and genetic studies suggest that histone acetylation plays an important role in the development of cardiac hypertrophy/heart failure (at least, in mouse), it is an open question whether changes in the other epigenetic marks are essential or, rather, causative of the heart disorders. An analysis of human heart specimens would be of particular great value.

In terms of technology development, DCS is not free from disadvantages. Although DCS can isolate genome fragments that are the recipients differential regulation of any epigenetic marks (provided specific antibodies are available), it does not measure the extent of "differential regulation". In other words, DCS is more a qualitative approach than a quantitative one. Several high-throughput sequencing technologies are currently emerging which simultaneously provide sequence information for millions of clones [21]. Coupling such sequencing system to ChIP would be one of the ideal ways to quantitatively measure epigenetic modifications: (1) frequency in the read data would be a surrogate marker for the intensity of epigenetic modifications; (2) sequence information of the reads would be useful to map such reads onto human genome.

It is apparent that epigenetic change is the key event in the development of cardiac hypertrophy/heart failure. Analysis of human specimens with emerging technologies would substantially facilitate researchers in their efforts to pinpoint the causative genes for these disorders.

References

1. Egger G, Liang G, Aparicio A, Jones PA. Epigenetics in human disease and prospects for epigenetic therapy. Nature. 2004;429:457–63.
2. Strahl BD, Allis CD. The language of covalent histone modifications. Nature. 2000;403:41–5.
3. Dion MF, Altschuler SJ, Wu LF, Rando OJ. Genomic characterization reveals a simple histone H4 acetylation code. Proc Natl Acad Sci USA. 2005;102:5501–6.
4. Verdin E, Dequiedt F, Kasler HG. Class II histone deacetylases: versatile regulators. Trends Genet. 2003;19:286–93.
5. Waterborg JH. Dynamics of histone acetylation in vivo. A function for acetylation turnover? Biochem Cell Biol. 2002;80:363–78.
6. Kouzarides T. Histone acetylases and deacetylases in cell proliferation. Curr Opin Genet Dev. 1999;9:40–8.
7. Yasui W, Oue N, Ono S, Mitani Y, Ito R, Nakayama H. Histone acetylation and gastrointestinal carcinogenesis. Ann NY Acad Sci. 2003;983:220–31.
8. Gusterson RJ, Jazrawi E, Adcock IM, Latchman DS. The transcriptional co-activators CREB-binding protein (CBP) and p300 play a critical role in cardiac hypertrophy that is dependent on their histone acetyltransferase activity. J Biol Chem. 2003;278:6838–47.
9. Iezzi S, Di Padova M, Serra C, Caretti G, Simone C, Maklan E, et al. Deacetylase inhibitors increase muscle cell size by promoting myoblast recruitment and fusion through induction of follistatin. Dev Cell. 2004;6:673–84.
10. Zhang CL, McKinsey TA, Chang S, Antos CL, Hill JA, Olson EN. Class II histone deacetylases act as signal-responsive repressors of cardiac hypertrophy. Cell. 2002;110:479–88.
11. Kook H, Lepore JJ, Gitler AD, Lu MM, Wing-Man Yung W, Mackay J, et al. Cardiac hypertrophy and histone deacetylase-dependent transcriptional repression mediated by the atypical homeodomain protein Hop. J Clin Invest. 2003;112:863–71.
12. Antos CL, McKinsey TA, Dreitz M, Hollingsworth LM, Zhang CL, Schreiber K, et al. Dose-dependent blockade to cardiomyocyte hypertrophy by histone deacetylase inhibitors. J Biol Chem. 2003;278:28930–7.
13. Kuwahara K, Saito Y, Ogawa E, Takahashi N, Nakagawa Y, Naruse Y, et al. The neuron-restrictive silencer element-neuron-restrictive silencer factor system regulates basal and endothelin 1-inducible atrial natriuretic peptide gene expression in ventricular myocytes. Mol Cell Biol. 2001;21:2085–97.
14. Weinmann AS, Yan PS, Oberley MJ, Huang TH, Farnham PJ. Isolating human transcription factor targets by coupling chromatin immunoprecipitation and CpG island microarray analysis. Genes Dev. 2002;16:235–44.
15. Ballestar E, Paz MF, Valle L, Wei S, Fraga MF, Espada J, et al. Methyl-CpG binding proteins identify novel sites of epigenetic inactivation in human cancer. EMBO J. 2003;22:6335–45.
16. Odom DT, Zizlsperger N, Gordon DB, Bell GW, Rinaldi NJ, Murray HL, et al. Control of pancreas and liver gene expression by HNF transcription factors. Science. 2004;303:1378–81.
17. Kaneda R, Toyota M, Yamashita Y, Koinuma K, Choi YL, Ota J, et al. High-throughput screening of genome fragments bound to differentially acetylated histones. Genes Cells. 2004;9:1167–74.
18. Kaneda R, Ueno S, Yamashita Y, Choi YL, Koinuma K, Takada S, et al. Genome-wide screening for target regions of histone deacetylases in cardiomyocytes. Circ Res. 2005;97:210–8.
19. Toyota M, Ho C, Ahuja N, Jair KW, Li Q, Ohe-Toyota M, et al. Identification of differentially methylated sequences in colorectal cancer by methylated CpG island amplification. Cancer Res. 1999;59:2307–12.
20. Marks AR. Cardiac intracellular calcium release channels: role in heart failure. Circ Res. 2000;87:8–11.
21. Service RF. Gene sequencing. The race for the $1000 genome. Science. 2006;311:1544–6.

Environ Health Prev Med (2008) 13:30–35
DOI 10.1007/s12199-007-0004-y

REVIEW

Epidemiological approach to nosocomial infection surveillance data: the Japanese Nosocomial Infection Surveillance System

Machi Suka · Katsumi Yoshida · Jun Takezawa

Received: 11 May 2007 / Accepted: 9 August 2007 / Published online: 11 December 2007

Abstract Surveillance of nosocomial infection is the foundation of infection control. Nosocomial infection surveillance data ought to be summarized, reported, and fed back to health care personnel for corrective action. Using the Japanese Nosocomial Infection Surveillance (JANIS) data, we determined the incidence of nosocomial infections in intensive care units (ICUs) of Japanese hospitals and assessed the impact of nosocomial infections on mortality and length of stay. We also elucidated individual and environmental factors associated with nosocomial infections, examined the benchmarking of infection rates and developed a practical tool for comparing infection rates with case-mix adjustment. The studies carried out to date using the JANIS data have provided valuable information on the epidemiology of nosocomial infections in Japanese ICUs, and this information will contribute to the development of evidence-based infection control programs for Japanese ICUs. We conclude that current surveillance systems provide an inadequate feedback of nosocomial infection surveillance data and, based on our results, suggest a methodology for assessing nosocomial infection surveillance data that will allow infection control professionals to maintain their surveillance systems in good working order.

Keywords Epidemiology · Intensive care units · Japan · Nosocomial infections · Surveillance

Introduction

Infection control in the hospital setting is performed with the aim of improving the effectiveness of patient care and promoting patient safety. Infection control professionals need to recognize and explain nosocomial infections and design and implement interventions to reduce their incidence. These infection control activities should have their bases in a well-designed surveillance system of nosocomial infections [1].

Compared with the USA and other developed countries, Japan traditionally had limited sources of information on the epidemiology of nosocomial infections and, until recently, little was known about the incidence and outcome of nosocomial infections in Japanese hospitals. The Japanese Ministry of Health, Labour, and Welfare established the Japanese Nosocomial Infection Surveillance (JANIS) system in July 2000, when participating hospitals routinely started to collect and subsequently make their nosocomial infection surveillance data available for entry into a national database. The JANIS database has now become the most important source of information on the epidemiology of nosocomial infections in Japanese hospitals.

In the study reported here, we used the JANIS data to determine the incidence of nosocomial infections in intensive care units (ICUs) of Japanese hospitals and assess the impact of nosocomial infections on mortality and length of stay. We elucidated individual and environmental

This article is based upon the research that was given encouragement award at the 77th annual meeting of the Japanese Society for Hygiene held in Osaka, Japan on 25–28 March 2007.

M. Suka (✉) · K. Yoshida
Department of Preventive Medicine, St Marianna University School of Medicine, 2-16-1 Sugao, Miyamae-ku Kawasaki, Kanagawa 216-8511, Japan
e-mail: suka@marianna-u.ac.jp

J. Takezawa
Department of Emergency and Intensive Care Medicine, Nagoya University Graduate School of Medicine, Nagoya, Japan

bjh research paper

Functional analysis of *JAK3* mutations in transient myeloproliferative disorder and acute megakaryoblastic leukaemia accompanying Down syndrome

Tomohiko Sato,[1] Tsutomu Toki,[1] Rika Kanezaki,[1] Gang Xu,[1] Kiminori Terui,[1] Hirokazu Kanegane,[2] Masayoshi Miura,[3] Souichi Adachi,[4] Masahiro Migita,[5] Shingo Morinaga,[6] Takahide Nakano,[7] Mikiya Endo,[8] Seiji Kojima,[9] Hitoshi Kiyoi,[10] Hiroyuki Mano[11] and Etsuro Ito[1]

[1]Department of Paediatrics, Hirosaki University Graduate School of Medicine, Hirosaki, [2]Department of Paediatrics, Graduate School of Medicine, University of Toyama, Toyama, [3]Department of Paediatrics, Toyama City Hospital, Toyama, [4]Department of Paediatrics, Graduate School of Medicine, Kyoto University, Kyoto, [5]Department of Paediatrics, Japan Red Cross Kumamoto Hospital, Kumamoto, [6]Department of Paediatrics, National Hospital Organization Kumamoto Medical Centre, Kumamoto, [7]Department of Paediatrics, Kansai Medical University, Osaka, [8]Department of Paediatrics, Iwate Medical University, Morioka, [9]Department of Paediatrics, Nagoya University Graduate School of Medicine, Nagoya, [10]Department of Infectious Diseases, Nagoya University Graduate School of Medicine, Nagoya, and [11]Division of Functional Genomics, Jichi Medical University, Shimotsuke, Japan

Summary

JAK3 mutations have been reported in transient myeloproliferative disorder (TMD) as well as in acute megakaryoblastic leukaemia of Down syndrome (DS-AMKL). However, functional consequences of the *JAK3* mutations in TMD patients remain undetermined. To further understand how *JAK3* mutations are involved in the development and/or progression of leukaemia in Down syndrome, additional TMD patients and the DS-AMKL cell line MGS were screened for *JAK3* mutations, and we examined whether each *JAK3* mutation is an activating mutation. *JAK3* mutations were not detected in 10 TMD samples that had not previously been studied. Together with our previous report we detected *JAK3* mutations in one in 11 TMD patients. Furthermore, this study showed for the first time that a TMD patient-derived *JAK3* mutation ($JAK3^{I87T}$), as well as two novel *JAK3* mutations ($JAK3^{Q501H}$ and $JAK3^{R657Q}$) identified in an MGS cell line, were activating mutations. Treatment of MGS cells and Ba/F3 cells expressing the JAK3 mutants with JAK3 inhibitors significantly decreased their growth and viability. These results suggest that the *JAK3* activating mutation is an early event during leukaemogenesis in Down syndrome, and they provide proof-of-principle evidence that JAK3 inhibitors would have therapeutic effects on TMD and DS-AMKL patients carrying activating *JAK3* mutations.

Keywords: Down syndrome, transient myeloproliferative disorder, acute megakaryoblastic leukaemia, JAK3, STAT5.

Received 14 November 2007; accepted for publication 2 January 2008
Correspondence: Etsuro Ito, Department of Paediatrics, Hirosaki University Graduate School of Medicine, Hirosaki, Aomori, 036-8563 Japan. E-mail: eturou@cc.hirosaki-u.ac.jp

Down syndrome (DS), which is caused by trisomy 21, is one of the most common human chromosomal abnormalities. Children with DS have an approximately 20-fold higher incidence of leukaemia than the general population (Hitzler & Zipursky, 2005). The majority of leukaemia cases associated with DS are acute megakaryoblastic leukaemia (AMKL). Approximately 10% of infants with DS develop a postnatal transient myeloproliferative disorder (TMD), which is characterized by rapid growth of abnormal blast cells with erythroid-megakaryocytic phenotype (Ito *et al*, 1995). Although the majority of TMD cases resolve spontaneously, AMKL develops in approximately 20% of TMD cases in the first four years of life. Recently, we and others demonstrated that acquired mutations of the *GATA1* gene were detected in almost all cases

 First published online 7 April 2008
British Journal of Haematology, **141**, 681–688 doi:10.1111/j.1365-2141.2008.07081.x

of DS-related AMKL (DS-AMKL) and TMD (Wechsler *et al*, 2002; Groet *et al*, 2003; Hitzler *et al*, 2003; Mundschau *et al*, 2003; Rainis *et al*, 2003; Xu *et al*, 2003; Ahmed *et al*, 2004). In each case, the mutation resulted in the introduction of a premature stop codon in the gene sequence encoding the N-terminal activation domain, leading to expression of an alternative 40-kD translation product (GATA1s) from a downstream initiation site.

The available evidence indicates that an acute leukaemia would arise from cooperation between one class of mutations that interferes with differentiation, such as loss-of-function mutations in haematopoietic transcription factors, and a second class of mutations that confers a proliferative advantage to cells, such as activating mutations in the haematopoietic tyrosine kinases (Deguchi & Gilliland, 2002). Indeed, Walters *et al* (2006) reported gain-of-function mutations of the *JAK3* gene in the DS-AMKL cell line CMK, and in one of three DS-AMKL patients, all of who also had *GATA1* mutations. These mutations consisted of A572V and V722I substitutions, which both occur in the JH2 pseudokinase domain. All JAK3 mutants constitutively activated and transformed Ba/F3 cells to factor-independent growth.

Recently, we identified a *JAK3* mutation in one of two TMD patients that were screened (Kiyoi *et al*, 2007). However, the functional consequences and frequency of the *JAK3* mutations in TMD patients remain undetermined. To further understand how *JAK3* mutations are involved in the development and/or progression of leukaemia in DS, we screened additional TMD patients as well as the DS-AMKL cell line MGS for *JAK3* mutations, and we examined whether each *JAK3* mutation is an activation mutation. *JAK3* mutations occurred in TMD patients at a low frequency, similar to that found earlier in DS-AMKL. Furthermore, we show for the first time that the previously identified $JAK3^{I87T}$ mutation associated with TMD, as well as two novel *JAK3* mutations ($JAK3^{Q501H}$ and $JAK3^{R657Q}$) identified in MGS cells, were activating mutations. Treatment of MGS cells and Ba/F3 cells expressing the JAK3 mutants with JAK3 inhibitors resulted in a significant decrease in their growth and viability. These results suggest that *JAK3* activating mutation is an early event during the development of AMKL in DS, and they provide proof-of-principle evidence that JAK3 inhibitors would have therapeutic effects on AMKL and TMD patients carrying activating *JAK3* mutations.

Materials and methods

Patients and cell lines

This study was approved by the Ethics Committee of Hirosaki University Graduate School of Medicine, and all clinical samples were obtained with informed consent. The MGS cell line was established from leukaemic cells obtained from a patient with DS-AMKL. This cell line was a gift from Dr. Mitsui (Yamagata University School of Medicine). The K562 cell line was established from leukaemic cells that were obtained from a patient with chronic myeloid leukaemia. These cell lines were cultured in RPMI 1640 medium (Sigma, St Lois, MO, USA) supplemented with 10% fetal bovine serum (Gibco BRL, Rockville, MD, USA). Ba/F3 cells were obtained from the Japanese Center Resources Bank and were cultured in RPMI 1640 medium supplemented with 10% fetal bovine serum and 1 ng/ml recombinant murine interleukin (IL)-3 (Kirin Brewery, Tokyo, Japan). PLAT-E, the retrovirus packaging cell line, was kindly provided by Dr Kitamura (the University of Tokyo; Morita *et al*, 2000). This cell line was cultured in Dulbecco's modified Eagle's medium (DMEM; Gibco BRL) supplemented with 10% fetal bovine serum and 1 μg/ml puromycin, 10 μg/ml brastidine, 50 U/ml penicillin and 50 μg/ml streptomycin. All cell lines were maintained at 37°C and in 5% CO_2 atmosphere.

Analysis of JAK3 mutations

To analyse *JAK3* mutation in clinical samples, total RNA was isolated from peripheral blood or bone marrow cells using an ISOGEN kit (Wako, Osaka, Japan) and was reverse transcribed using random hexamers. The synthesized cDNA were amplified using a ligation-anchored polymerase chain reaction (LA PCR) kit (TaKaRa, Ohtsu, Japan) and direct sequencing was performed by means of the ABI PRISM Bigdye Terminator Cycle Sequencing Ready Reaction Kit (Applied Biosystems, Foster City, CA, USA). The primers used in this analysis are shown in Table SI. To analyse *JAK1* mutation in MGS cells, direct sequence analysis for the entire coding sequences was performed using cDNA.

Construction of retroviral vectors

To establish each retroviral expression vector, the pMX-ires-CD8 plasmid vector (Yamashita *et al*, 2001) was used. The wild type *JAK3* cDNA was ligated into the *Eco*RI site of pMX-ires-CD8 to produce pMX-ires-CD8-$JAK3^{WT}$. The other retroviral expression vectors, pMX-ires-CD8-$JAK3^{Q501H}$, pMX-ires-CD8-$JAK3^{R657Q}$, pMX-ires-CD8-$JAK3^{Q501H\ and\ R657Q}$, pMX-ires-CD8-$JAK3^{A572V}$ and pMX-ires-CD8-$JAK3^{V674A}$ were generated from pMX-ires-CD8-$JAK3^{WT}$ by PCR.

Ba/F3 cell transformation assay

PLAT-E cells were transfected with plasmid DNA using the Fugene transfection kit (Roche, Basel, Switzerland). Retroviral supernatants were collected 72 h after transfection and incubated with Ba/F3 cells for 24 h in the RetroNectin Dish (TaKaRa). To obtain the transduced cells, CD8-positive cells were selected using a MACS Separation Column (Miltenyi Biotec, Bergisch Gladbach, Germany) and expanded. Finally, we confirmed the transductions by detecting CD8-positive cells using fluorescence-activated cell sorting (FACS).

Cell proliferation assay

Ba/F3 cells expressing JAK3 mutants were incubated in the absence of IL-3 for 7–8 days. Viable cell number was determined every 1–2 days using Cell Counting Kit 8 (Wako, Osaka, Japan), according to the manufacturer's recommendations.

Immunoblot analysis

Before obtaining whole-cell extracts, Ba/F3 cells were cultured in serum-free RPMI 1640 medium for 4 h and then incubated in medium with 10% fetal bovine serum for 5 min. The whole-cell extracts were separated on SDS-PAGE and transferred to Hybond-P membranes (Amersham Biosciences, Little Chalfont, UK). Immunodetections were carried out using anti-phospho-STAT5 (Cell Signalling, Danvers, MA, USA) and anti-STAT5 antibodies (Santa Cruz Biotechnology, Santa Cruz, CA, USA). Dilutions were 1:1000 and 1:500 respectively. The signals were visualized with anti-rabbit horseradish peroxidase conjugates (GE Healthcare UK LTD, Buckinghamshire, England) and enhanced chemiluminescence (ECL) plus Western blotting detection reagents (Amersham Biosciences).

JAK inhibitors assay

For the purpose of the inhibitor analysis, Ba/F3 cells expressing various JAK3 mutants were cultured for 10 days in the absence of IL-3. These cells were treated with increasing concentrations of WHI-P131 (JAK3 inhibitor I) and WHI-P154 (JAK3 inhibitor II). After 48 h, the viable cell number was determined using Cell Counting Kit 8.

Results

JAK3 mutations in the DS-AMKL cell line MGS

To investigate the role of the JAK/STAT pathway in DS-associated leukaemogenesis, we first examined the effects of a pan-JAK inhibitor on the growth and viability of the DS-AMKL cell line MGS. Treatment with the pan-JAK inhibitor (JAK inhibitor I) resulted in significantly decreased cell proliferation and viability (Fig 1A). This effect could not be attributed to nonspecific toxicity, because growth and viability were not inhibited by pan-JAK inhibitor in K562 cells that express the BCR-ABL fusion protein. These results suggest that JAK activation was essential for growth and survival of MGS cells. Because reverse transcription (RT)-PCR analysis showed that, of the JAK family, only *JAK1* and *JAK3* were expressed in MGS cells (data not shown), we then analysed *JAK1* and *JAK3* for activating mutations. Sequence analysis identified two novel *JAK3* mutations (a Q501H substitution in the JH3 SH2 domain and an R657Q substitution in the JH2 pseudokinase domain) in MGS cells (Fig 1B and C), whereas no mutation was detected in *JAK1*. We performed RT-PCR analysis using primers corresponding to the outside of each mutation. A PCR product encompassing both mutations was

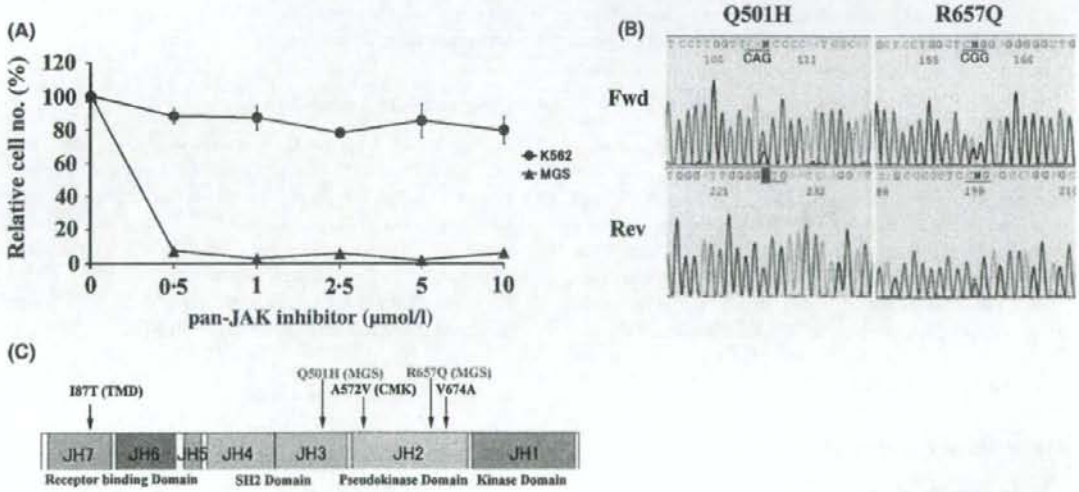

Fig 1. *JAK3* mutation in the DS-AMKL cell line MGS. (A) Treatment with the pan-JAK inhibitor (JAK inhibitor I) resulted in significantly decreased cell proliferation and viability of MGS cells, but not K562 cells that express the BCR–ABL fusion protein. Viable cell number was determined using Cell Counting Kit 8 at 72 h. Mean value ± SD of experiments performed in triplicate is represented. For each cell line, the relative cell number in presence of increasing amount of inhibitor was calculated as a percentage of control (without inhibitor). (B) Sequence analysis of the *JAK3* gene showing that MGS cells harbour two novel mutations (Q501H and R657Q) in the same allele. (C) Q501H and R657Q, indicated by red letters, were located in the JH3 SH2 domain and JH2 pseudokinase domain respectively. A572V, identified in CMK cells, and the artificially generated V674A were located in the pseudokinase domain, and the I87T associated with the TMD patient and indicated by black letters occurred in the receptor-binding domain.

cloned into plasmid pCR II (Invitrogen). Sequence analysis confirmed that the two mutations were in the same allele.

JAK3 contains a gain-of-function mutation in MGS cells

To examine the transforming ability of *JAK3*^{Q501H} and *JAK3*^{R657Q} mutations, we constructed retroviral expression vectors containing various *JAK3* mutations and transduced Ba/F3 cells with either pMX-ires-CD8-*JAK3*^{Q501H}, *JAK3*^{R657Q}, *JAK3*$^{Q501H\ and\ R657Q}$ or *JAK3*^{WT}. As positive controls, we used the expression vectors pMX-ires-CD8-*JAK3*^{A572V} for the JAK3 activating mutation identified in CMK and pMX-ires-CD8-*JAK3*^{V674A} for the artificially generated, oncogenic *JAK3* mutation (Choi *et al*, 2006; Walters *et al*, 2006). Twenty-four hours after transduction, CD8-positive cells were selected using immunobeads, cultured in the absence of IL-3, and subjected to the cell proliferation assay. As shown in Fig 2A, expression of either JAK3^{Q501H} or JAK3^{R657Q} conferred IL-3-independent growth to Ba/F3 cells, but these cells grew much more slowly than the Ba/F3 cells expressing JAK3^{V674} or JAK3^{A572V}. Interestingly, the cells transduced with pMX-ires-CD8-*JAK3*$^{Q501H\ and\ R657Q}$ grew as fast as the positive controls, suggesting that the JAK3$^{Q501H\ and\ R657Q}$ showed more potent transforming activity than did either single substitution.

Constitutive and ligand-independent activation of the downstream signalling pathway induced by JAK mutations

To analyse signalling properties of the JAK3 mutants, we next evaluated the phosphorylation status of STAT5, the downstream target of JAK3. Western blot analysis of Ba/F3 cells revealed that STAT5 was constitutively phosphorylated in cells transduced with JAK3$^{Q501H\ and\ R657Q}$ or with JAK3^{V674} or JAK3^{A572V}, but not in cells transduced with JAK^{WT}. STAT5 phosphorylation was also detected in cells transduced with JAK3^{Q501H} or JAK3^{R657Q}, but this effect was very weak compared with JAK3$^{Q501H\ and\ R657Q}$ (Fig 2B). These results suggest that the transforming activity is correlated with the kinase activity of each JAK3 mutant protein.

JAK3 mutation identified in a TMD patient

We previously found *JAK3* mutations in one of two TMD and one of 11 DS-AMKL patients (Kiyoi *et al*, 2007). The A573V and A593T substitutions, which occur in the same allele and which both are in the JH2 pseudokinase domain, were found in the one affected DS-AMKL patient, while the affected TMD patient had an I87T substitution in the JH7 receptor-binding domain. Of note, the fact that the *JAK3* mutation was found in a TMD patient indicated that this is an early event during the development of AMKL in DS. However, the frequency and functional consequences of *JAK3* mutations in TMD remain unknown because of the small sample size. We therefore screened for *JAK3* mutations in another 10 TMD patients by analysing their cDNA. Direct sequence analysis revealed no *JAK3* mutations in these patients, while *GATA1* mutations were detected in all cases (Table I). Recently, De Vita *et al* (2007) reported an acquired loss-of-function *JAK3* mutation because of a large deletion (592 bp) of a fragment encoding the JH1 kinase domain. This mutation was found in two of eight TMD patients and in one of eight DS-AMKL patients (De Vita

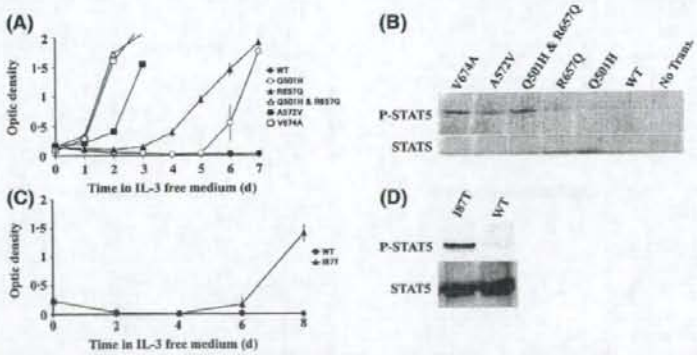

Fig 2. *JAK3* mutations from MGS cells and a TMD patient transformed Ba/F3 cells. (A) Expression of JAK3 mutants identified in MGS cells abrogated cytokine dependency of Ba/F3 cells. Ba/F3 cells were transduced with either pMX-ires-CD8-*JAK3*^{Q501H}, *JAK3*^{R657Q}, *JAK3*$^{Q501H\ and\ R657Q}$ or *JAK3*^{WT}. Positive controls were pMX-ires-CD8-*JAK3*^{A572V} for the JAK3-activating mutant identified in CMK cells and pMX-ires-CD8-*JAK3*^{V674A} for the artificially-generated oncogenic JAK3 mutant (Choi *et al*, 2006; Walters *et al*, 2006). After transduction, CD8-positive cells were selected using immunobeads, cultured at a density of 2×10^5/ml in the absence of IL-3 and evaluated by a cell proliferation assay. Values represent mean ± SD. The experiments were repeated twice, and both data sets were essentially identical. (B) *JAK3* mutations cause constitutive JAK3 activation. Ba/F3 cells were transduced with various JAK3 expression vectors, and CD8-positive cells were selected using immunobeads. Cell lysates were subjected to immunoblot analysis for phospho-STAT5 and total STAT5. (C) Ba/F3 cells were transduced with either pMX-ires-CD8-*JAK3*^{I87T} or *JAK3*^{WT}. After transduction, CD8-positive cells were selected using immunobeads, cultured at a density of 4×10^5/ml in the absence of IL-3, and evaluated by a cell proliferation assay. Values represent mean ± SD. The experiments were repeated twice, and both data sets were essentially identical. (D) Ba/F3 cells expressing JAK3^{I87T} were grown in the absence of IL-3. Lysates of Ba/F3 cells were subjected to immunoblot analysis for phospho-STAT5 or total STAT5.

Table I. Mutations of *GATA1* and *JAK3* genes in transient myeloproliferative disorder (TMD) patients.

Patients	Sex	Blast (%)	*GATA1* mutations	*JAK3* mutations
TMD-1	Male	82	Exon 2, subs 7, pos 305	Wild
TMD-2	Female	86	Exon 2, del 2, pos 202	Wild
TMD-3	Male	92	Exon 2, ins 12, pos 298	Wild
TMD-4	Male	69	Exon 2, subs (T > C) exon/intron boundary	Wild
TMD-5	Male	84	Exon 3, del 129, pos 342	Wild
TMD-6	Female	48	Exon 2, del 136, pos 94	Wild
TMD-7	Male	93	Exon 2, del 23, pos 265	Wild
TMD-8	Male	94	Exon 2, del 218, exon/intron boundary	Wild
TMD-9	Female	55	Exon 2, subs (C > G) pos 319	Wild
TMD-10	Male	60	Exon 2, del 8, pos 213	Wild

del, deletion; subs, substitution; ins, insertion.
Nucleotide position 1 is taken from GenBank sequence of human *GATA1* (NM_002049).

et al, 2007). However, we failed to detect these mutations in any of our patients.

To examine whether the $JAK3^{I87T}$ mutation identified in a TMD patient was an activating mutation, Ba/F3 cells were transduced with either pMX-ires-CD8-$JAK3^{I87T}$ or $JAK3^{WT}$. As shown in Fig 2C, expression of JAK^{I87T} conferred IL-3-independent growth to Ba/F3 cells, whereas $JAK3^{WT}$-transduced cells retained dependence on IL-3 for proliferation. However, these cells grew slower than the Ba/F3 cells expressing either $JAK3^{Q501H}$, or $JAK3^{R657Q}$ (data not shown). The constitutive phosphorylation of STAT5 was weaker in the cells expressing JAK^{I87T} than $JAK3^{Q501H}$ or $JAK3^{R657Q}$ (data not shown), and was detected only after JAK^{I87T}-transduced cells started growing in the absence of IL-3 (Fig 2D). These results suggest that $JAK3^{I87T}$ is a gain-of-function mutation, although its kinase activity was weak compared with that associated with the other JAK3 mutants.

JAK3 inhibitors affect the proliferation of cells expressing JAK3 mutants

We next assessed the effects of small molecule JAK inhibitors on the proliferation of MGS cell expressing JAK3 mutant proteins. Treatment with WHI-P154 (JAK3 inhibitor II), but not the JAK2 inhibitor AG490, resulted in significantly decreased proliferation of MGS cells compared with K562 cells (Fig 3A and B). To further study the effects of JAK3 inhibitors on each JAK3 mutant, we next examined the effects

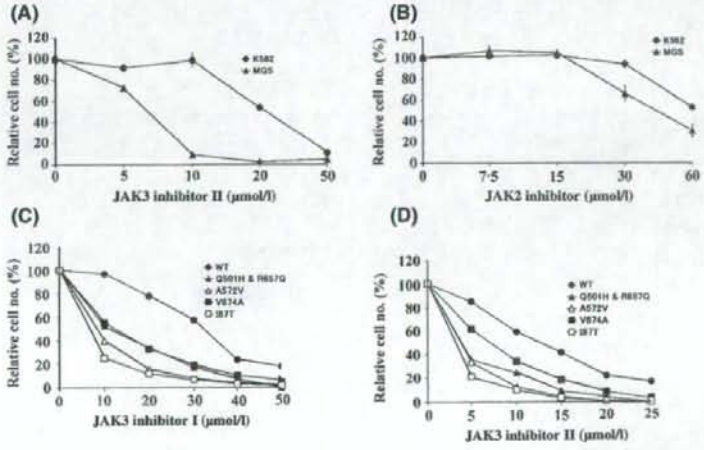

Fig 3. JAK3 inhibitors affect proliferation of cells expressing JAK3 mutants. MGS and K562 control cells were treated with increasing concentrations of WHI-P154 (JAK3 inhibitor II) (A) or JAK2 inhibitor AG490 (B). Note that treatment with WHI-P154, but not AG490, resulted in significantly decreased proliferation of MGS cells compared with K562 cells. Ba/F3 cells expressing various JAK3 mutants without added IL-3 and Ba/F3 cells expressing $JAK3^{WT}$ with added IL-3 were treated with increasing concentrations of WHI-P131 (JAK3 inhibitor I) (C) or JAK3 inhibitor II (D). Viable cell number was determined using Cell Counting Kit 8 at 48 h. Mean value ± SD of experiments performed in triplicate is represented. For each cell line, the relative cell number in presence of increasing amount of inhibitor was calculated as a percentage of control (without inhibitor). The experiments were repeated twice, and both data sets were essentially identical.

of JAK inhibitors on the Ba/F3 cells expressing each JAK3 mutant. For this analysis, Ba/F3 cells expressing various JAK3 mutants were cultured for 10 days in the absence of IL-3. These cells grew slowly at first, as shown in Fig 2A and C. However, they all started growing well in the absence of IL-3 subsequently. WHI-P131 (JAK3 inhibitor I) and JAK3 inhibitor II inhibited the proliferation of all Ba/F3 cells expressing the various JAK3 mutants in the absence of IL-3, although the sensitivities to each JAK3 inhibitor differed slightly among these Ba/F3 cells (Fig 3C and D and Fig S1). This effect could not be attributed to nonspecific toxicity, because the sensitivities to the Ba/F3 cells expressing $JAK3^{WT}$ were significantly reduced in the presence of IL-3, whose receptor utilizes JAK2 (Silvennoinen *et al*, 1993). These results confirmed that the gain-of-function mutations of *JAK3* conferred IL-3 independent growth to Ba/F3 cells.

Discussion

Analysis of TMD and DS-AMKL may provide invaluable information for understanding leukaemia pathogenesis. To further understand how *JAK3* mutations are involved in the development and/or progression of leukaemia in DS, we screened TMD patients and the DS-AMKL cell line MGS for *JAK3* mutations and examined the functional consequences of these mutations. This study showed, for the first time, that a TMD patient-derived *JAK* mutation ($JAK3^{I87T}$), as well as two novel *JAK3* mutations ($JAK3^{Q501H}$ and $JAK3^{R657Q}$) identified in an MGS cell line, were activating mutations. These results have significantly improved our understanding of the mechanisms of multi-step leukaemogenesis in DS.

Only two DS-AMKL cell lines, CMK and MGS, have been reported until now. *GATA1* mutations were detected in both of these cell lines (Xu *et al*, 2003). The results are consistent with the fact that *GATA1* mutations are detected in almost all cases with TMD and DS-AMKL. Furthermore, we identified the mutations of the *TP53* tumour suppressor genes in both of these cell lines (Kanezaki *et al*, 2006). However, the roles of *TP53* mutations in DS-AMKL remain unknown, because *TP53* mutations are rare in DS-AMKL as well as TMD (Hirose *et al*, 2003) and the inactivation of p53 is frequently observed in myeloid leukaemia cell lines. Recently, Walters *et al* (2006) first reported *JAK3* activating mutations (A572V) in CMK cells. This study identified two novel *JAK3* activating mutations (Q501H and R657Q in the same allele) in MGS cells. The fact that two out of two DS-AMKL cell lines have activating *JAK3* mutations indicates that constitutive activation of the JAK/STAT pathway may play a very important role in the development of leukaemia in DS.

An activating *JAK2* mutation affecting the pseudokinase domain ($JAK2^{V617F}$) has been observed frequently in myeloproliferative disorders (Baxter *et al*, 2005; James *et al*, 2005; Levine *et al*, 2005). In contrast to the *JAK2* mutations, *JAK3* mutations have been observed in a variety of domains including the JH2 pseudokinase domain, the JH3 SH2 domain and the JH6 and JH7 receptor binding domain (Choi *et al*, 2006; Walters *et al*, 2006; De Vita *et al*, 2007; Kiyoi *et al*, 2007). However, only four activating JAK3 mutants, including one artificially generated mutant, were verified using functional assays (Choi *et al*, 2006; Walters *et al*, 2006). Among these four mutations, three were located in the JH2 pseudokinase domain and the remaining mutation was located in the JH6 receptor-binding domain. The SH2 domain is thought to contribute to *in vivo* assembly of the JAK, but the functional role of this domain is only partly defined. This study showed, for the first time, that a mutation in the SH2 domain ($JAK3^{Q501H}$) was also an activating mutation. Interestingly, the double mutation $JAK3^{Q501H \text{ and } R657Q}$ had much more potent transforming activity than did each individual substitution, but the mechanism behind this effect remains unknown. We used the Ba/F3 transformation assay to examine whether each JAK3 mutant is an activating mutation. This is a standard assay *in vitro* but of limited value. JAK3 mutants are expressed at non-physiological levels in a myelo-lymphoid cell line rather than primary cells that have a megakaryocyte-erythroid phenotype. To further understand the roles of *JAK3* mutations in leukaemogenesis, it is necessary to express JAK3 mutants in primary bone marrow cells *in vitro* and *in vivo*.

Our findings, taken together with previous published data (Walters *et al*, 2006; De Vita *et al*, 2007; Kiyoi *et al*, 2007; Klusmann *et al*, 2007; Norton *et al*, 2007), show that the observed incidence of *JAK3* mutations in TMD and in DS-AMKL was 5/38 patients and 6/45 patients respectively. Although the incidences of *JAK3* mutations in TMD and DS-AMKL differ from reports in three other recent studies (De Vita *et al*, 2007; Klusmann *et al*, 2007; Norton *et al*, 2007), these results indicate that the frequency of *JAK3* mutations in TMD and DS-AMKL is similar. This suggests that *JAK3* mutations are very early events that can cooperate with *GATA1* mutations during the development of TMD. However, the fact that *JAK3* mutations occurred in TMD patients and in DS-AMKL patients only at a low frequency suggests that other distinct genetic changes probably contribute to the development of TMD, and to the progression to AMKL from TMD.

This study has shown for the first time that a TMD patient-derived *JAK* mutation was also an activating mutation. The N-terminal portion of the JAK3 JH5-JH7 domain, which has homology to a band four-point-one, ezrin, radixin, soesin (FERM; Girault *et al*, 1999), is required for receptor binding and maintenance of a functional kinase domain (Zhou *et al*, 2001). Severe combined immunodeficiency (SCID) patient-derived mutations within the JAK3 FERM domain impair the kinase-receptor interaction and abrogate JAK3 catalytic activity. In this study, we showed that the TMD patient-derived $JAK3^{I87T}$, which leads to an amino-acid substitution in the JH7 FERM domain, is an activating mutation, like the substitution $JAK3^{P132T}$, which was found in a non-DS-AMKL patient (Walters *et al*, 2006).

Functional analysis of *JAK3* mutations in this study indicates the possibility that *JAK3* mutations are the cause of